# Identification of a Selectivity Determinant for Inhibition of Tumor Necrosis Factor-α Converting Enzyme by Comparative Modeling

Zelda R. Wasserman,[1,3,*] James J.-W. Duan,[2]
Matthew E. Voss,[2] Chu-Biao Xue,[2,3]
Robert J. Cherney,[2] David J. Nelson,[2]
Karl D. Hardman,[1] and Carl P. Decicco[2,*]
[1] Structural Biology and Molecular Design Group
[2] Discovery Chemistry
Bristol-Myers Squibb Company
Experimental Station
Wilmington, Delaware 19880

## Summary

Inhibition of tumor necrosis factor-α converting enzyme (TACE) is a widespread objective in the search for disease modifying agents to combat rheumatoid arthritis and other autoimmune diseases. Until recently, most of the inhibitors in the literature have shown concomitant activity against the related matrix metalloproteinases (MMPs), producing undesired side effects. Here we describe the successful search for a TACE selectivity mechanism. We built a homology model based on the crystal structure of the related snake venom protein atrolysin. Comparison of the model with crystal structures of MMPs suggested a uniquely shaped S1′ pocket that might be exploited for selectivity. A novel γ-lactam scaffold [1] was used to explore the activity profile of P1′ sidechains, resulting in highly selective compounds consistent with this hypothesis. Transferability of the hypothesis was then demonstrated with five other distinct scaffolds.

## Introduction

Tumor necrosis factor-α (TNF-α), a proinflammatory cytokine, is a key mediator of inflammatory disorders such as rheumatoid arthritis (RA) and Crohn's disease. In 1994, studies by Centocor and the Kennedy Institute demonstrated the striking effect of an anti-TNF-α antibody (cA2) in treating rheumatoid arthritis patients [2]. This humanized antibody now known as infliximab and the TNFR II receptor fusion protein etanercept have gained approval as therapeutics for the treatment of RA and Crohn's disease [3, 4]. The validation of TNF-α as a therapeutic target by these systemically injectable macromolecules has led to a number of small-molecule approaches to inhibition of this cytokine [5].

Gearing and coworkers at British Biotech discovered that the precursor of TNF-α (pro-TNF-α) was processed to the soluble form through the action of a metalloproteinase [6]. In addition, TNF-α release from cells could be inhibited by small-molecule metalloproteinase inhibitors. These findings suggested an attractive small-molecule enzymatic target for drug design. Subsequently

*Correspondence: zeldaw@incyte.com (Z.R.W.), carl.decicco@bms.com (C.P.D.)
[3] Present address: Incyte Genomics, Inc., 1090 Elkton Road, Newark, Delaware 19711.

Black and colleagues at Immunex [7] and Moss and colleagues at Glaxo [8] reported the identification of a new metalloproteinase termed TACE (TNF-alpha converting enzyme) that effectively cleaves the 26 kDa pro-TNF-α to the soluble 17 kDa protein.

TACE, a member of the ADAM (a disintegrin and metalloproteinase) family of enzymes, has sequence similarity to the reprolysin or snake venom family of metalloproteinases [7]. The importance of this enzyme as a therapeutic target was supported by the positive data, generated in in vitro and in vivo models of inflammatory disease, using previously identified matrix metalloproteinase (MMP) inhibitors that also inhibit TACE. While these inhibitors are important tools for biological discovery, they are not suitable for drug development. A major flaw in their profile may be the broad spectrum of activity against related metalloproteinases, primarily members of the matrix metalloproteinases. The MMPs are a large family of enzymes (>20 currently known) involved in both normal and pathological processes primarily associated with degradation and remodeling of macromolecules contained in the extracellular matrix. While it is possible that the broad spectrum (TACE plus MMP) inhibitory activity of the initial TACE leads may contribute to the overall efficacy of these molecules, their nonselective profile greatly increases the possibility of inducing undesirable side effects on prolonged dosing in animals or humans. For example, broad-spectrum MMP inhibitors such as marimastat [9], prinomastat [10], and CGS27023A [11] have been associated with the side effect of musculoskeletal pain in human clinical trials.

Comparison of the protein sequence of TACE with MMPs reveals low overall homology but high sequence similarity in the active site regions of the enzymes. It is likely the reason that identification of selective inhibitors of TACE proved elusive until recently [12, 1, and references therein]. It was our intention to identify selective inhibitors of TACE that could be used to evaluate the dependence of TNF-α processing on this single enzyme and, more importantly, to evaluate the efficacy and therapeutic potential of such inhibitors in vivo. This report details our use of computer-assisted drug design, based on sequence information of TACE and publicly available X-ray crystallographic structures of MMPs and snake venom proteins, in the development of selective inhibitors of TACE. Of significance, we demonstrate how sequence information across a family of closely related enzymes can be combined with comparative modeling of the target enzyme to identify the regions to exploit in attaining selectivity. The derivation of a TACE homology model, pinpointing of key active site regions, and selection of appropriate chemical substituents to maximize TACE inhibition while sparing the activity of closely related enzymes are described.

## Results and Discussion

### Sequence Similarity

Reprolysins and MMPs belong to the metzincin family of zinc endoproteinases whose catalytic site contains

a zinc ion coordinated by three histidines. Just below this active site is located a conserved methionine residue which gives name to the family. The metzincins are zymogens, having an N-terminal propeptide which must be cleaved in order to activate their catalytic domains. All except MMP-7 contain a hemopexin-like domain C-terminal to the catalytic portion. In addition, the gelatinases MMP-2 and MMP-9 have a fibronectin-like insertion within the catalytic domain [13].

The sequences of MMP-1, -2, -3, -8, and -9 were aligned, as were a representative set of reprolysins (see Experimental Procedures). The catalytic domains of the MMPs are very similar, with approximately 55%–65% sequence identity, so despite short insertions, the sequences could be aligned unambiguously. The set of reprolysins is at least as similar. For example, 80% of the residues of the catalytic domains of adamalysin and atrolysin are identical.

TACE contains the zinc binding motif HExxHxxGxxH characteristic of metzincins, as well as their conserved triplet MxP. Apart from these two segments, we could detect essentially no sequence similarity between TACE and MMPs. We did find almost 30% identity between TACE and the reprolysin family, but alignment was complicated by the fact that the sequences of the catalytic domains were of unequal length (TACE having an additional 56 residues), and even approximate locations of the necessary insertions could not in all cases be determined based on sequence alone.

## Building the Homology Model

Many of the known MMP inhibitors are also highly effective against TACE. It was therefore conjectured that the enzyme active sites must have structural similarity. This belief was reinforced by the sequence analysis, because in crystal structures the active site sequence motifs of reprolysins and MMPs are superimposable. Our intent was to create a model of TACE that would drive the identification of inhibitors highly selective for the enzyme. The medicinal chemistry effort in our laboratory was, at that time, targeted on P3′ and P4′ (notation of Schechter and Berger [14]) as determinants of selectivity, so we particularly wanted to focus on the composition and conformation of the protein segments forming S3′ and S4′ of TACE.

Both the MMP and reprolysin families exhibit a characteristic topology consisting of a five-stranded β sheet and three α helices [15]. The enzymes are organized into two domains, an upper consisting of the β sheet and two α helices and a lower containing the third helix as well as the MxP triplet and the following 8–10 residues, which form the outer side of S1′ and are known as the P1′ loop. MMPs bind a second, structural zinc in addition to the catalytic one and a number of structural calcium ions while reprolysins have no additional zinc or other metal binding sites [16]. Whereas the catalytic domains of the MMPs have no disulfides, both atrolysin and adamalysin (the reprolysins whose structures have been determined [17, 18]) contain two disulfide bridges [16], and TACE has six cystine residues.

In accord with their very similar sequences, atrolysin (*1htd.pdb*) and adamalysin (*1iag.pdb*) have essentially identical three-dimensional structures. Thus we felt there was little to be gained in basing a model on more than one homolog and made the arbitrary choice of atrolysin as a model for TACE. The initial alignment of the two sequences was taken from a multiple one of TACE and a set of reprolysins. An iterative process of model generation, model inspection, and alignment modification followed (see Experimental Procedures). Since 25% of the identical residues fall within the catalytic site region, and because of the large number of inserted residues in TACE, there were numerous ways in which the sequences could be aligned while still maintaining about 29% sequence identity. As the process of model generation progressed, stretches of sequence similarity became concentrated into segments for which atrolysin displayed well-defined secondary structure. Our final alignment is shown in Figure 1. A sequence alignment of adamalysin with TACE, in which several of the β strands are aligned differently, was subsequently published by Gomis-Ruth et al. [19].

The C-terminal domain was easier to align than the larger N-terminal one. Early on in the model-building process, we identified a disulfide bridge between Cys204 and Cys234 (numbering from Pro1 to Ser255; see Figure 1). Concentrating our model optimization efforts on the characteristic β sheet and three helices, and on loops abutting the prime side of the active site groove, we made little attempt to optimize the other faces of the globular structure. We reasoned that with so many inserted residues, a model which is accurate everywhere is unlikely to be achieved and that we should therefore concentrate on the core of the protein and loops at the active site. In our final alignment, three of the six cystine residues occur in, or on the edge of, inserted segments. Because of this, we did not predict which of the four unpaired cystine residues would link with each other, although we were convinced all six would form disulfide bonds.

## Analysis of the Homology Model

The atomic structures and molecular surfaces of the TACE model and MMP crystal structures were inspected to identify opportunities for incorporating selectivity into inhibitors. Although we had hoped to locate opportunities for selective inhibition at S3′ and S4′, comparison of the TACE model with MMP structures indicated the most striking difference to be their S1′ pockets. In MMP-3, S1′ extends straight back from the protein surface, whereas that of the TACE model exhibits a distinctly curved shape. S1′ of MMP-1 is foreshortened by an arginine side chain and MMP-8's by another arginine 6 or 7 Å deeper into the pocket, but both are otherwise similar to that of MMP-3.

To probe the suggested difference in pocket size and shape, we utilized the crystal structure of MMP-3 inhibited by a molecule having a biphenyl moiety at P1′ [20]. This complex was chosen because the inhibitor's P1′ substituent was the longest of those in MMP/inhibitor crystal structures known to us at that time. Although the zinc-chelating unit is a carboxylic acid rather than the more common hydroxamic acid, it had been shown that the two can bind in an identical fashion [21].

Figure 1. Sequence Alignment of Atrolysin and TACE Used in Building the Homology Model

Identical amino acid residues are highlighted in yellow, similar pairs in green. Secondary structural assignments for Atrolysin were taken from Protein Data Bank entry *1htd* and are indicated above the sequence. Segments of TACE that were modeled correctly, in the sense that the model and crystal structure superimpose, are indicated by blue lines.

Thus, assuming that inhibitors would bind similarly in MMPs and TACE, we overlaid the model of TACE with the crystal structure of MMP-3 by superimposing C-alphas of residues of the catalytic site HExxHxxGxxH motif and examining the molecular surfaces of the pockets and their orientation with respect to the inhibitor (Figure 2). In the crystal structure of inhibited MMP-3, S1′ is a linear tunnel with the biphenyl centered within (Figure 2A); the inhibitor binds to MMP-3 with $K_i = 21$ nM. In the superimposed TACE model, S1′ has a distinctly bent shape (Figure 2B), and the distal ring collides with the pocket wall; when tested in TACE, the inhibitor was inactive.

Rationale for the difference in shape is suggested by comparison of the sequences (Figure 3). In MMPs, the second residue following the MxP triplet is tyrosine, conserved in all known members of the family. As early as 1994, an NMR study of inhibited MMP-3 by Gooley and colleagues [22] had identified this tyrosine as contacting P1′ and forming one side of S1′. For reprolysins, the equivalent position is occupied by a smaller residue such as isoleucine or leucine. In TACE, there is an ala-nine, a very small residue that may open the side of the pocket to solvent (Figure 4).

These observations strongly suggested (1) that selectivity could be achieved by suitable modification of P1′ and (2) that the designated substituent should have, or should be able to adopt, a bent conformation.

### Discovery of TACE-Selective P1′ Groups

The search for selective TACE inhibitors started with a novel γ-lactam hydroxamate scaffold, designed from the structure of MMP-3 and MMP inhibitors reported in the literature [1, and references therein]. One of the early analogs, biphenyl lactam **1a**, was only weakly active in pTACE and MMP-1 (Table 1), but potent for MMP-2 and -9 (with $K_i$'s of 82 and 35 nM, respectively). Based on computer analysis described above (see Analysis of the Homology Model), we conjectured that the rigid 4-biphenyl group of **1a** would occupy the deep and linear S1′ pocket of MMP-2 and -9 while being too long to fit into the shallow S1′ of MMP-1. The lack of TACE potency had been anticipated because it was in accord with our conformational hypothesis of a curved S1′.
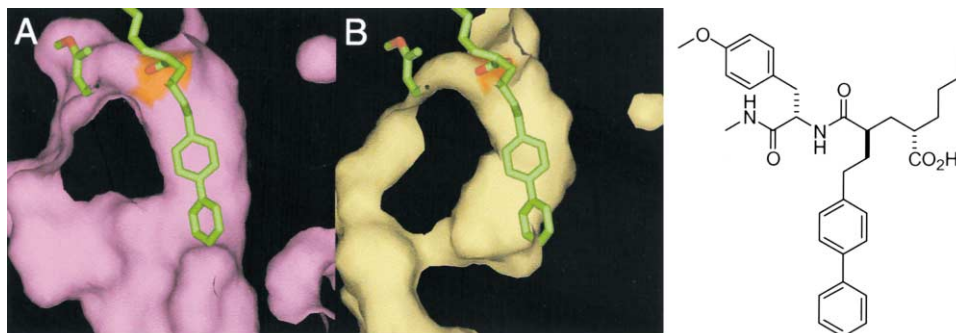


Figure 2. Slice through the Center of (A) the Crystal Structure of the MMP-3/Inhibitor Complex and (B) Inhibitor with the Homology Model of TACE

(B) was made by overlaying the catalytic site residues of the TACE model with those of the MMP-3 crystal structure. In (B), MMP-3 is not shown. The structure of the inhibitor is given in approximately the same orientation as in the models.

```
mmp2_human    VAAHEFGHAMGLEHSQDP............GALMAPIY
mmp9_human    VAAHEFGHALGLDHSSVP............EALMYPMY
mmp8_human    VAAHEFGHSLGLAHSSDP............GALMYPNY
mmp1_human    VAAHELGHSLGLSHSTDI............GALMYPSY
mmp3_human    VAAHEIGHSLGLFHSANT............EALMYPLY

      tace    VTTHELGHNFGAEHDPDGLAECAPNEDQGGKYVMYPIA

adamalysin    TMAHELGHNLGMEHDGKD.....CLR.GASLCIMRPGL
  atrolysin   TMAHELGHNLGMEHDGKD.....CLR.GASLCIMRPGL
  jararhagin  IMAHEMGHNLGIHHDTGS.....CSC.GDYPCIMGPTI
trimerelysin  IMTHEMGHNLGIPHDGNS.....CTC.GGFPCIMSPMI
   trigramin  TMTHEMGHNLGMHHDEDK.....CNC.N..TCIMSKVL
 rhodostomin  IMAHEMGHNLGVRHDGEY.....CTCYGSSECIMSSHI
```

Figure 3. Alignment of Sequences of MMP and Reprolysin Family Members with TACE

Shown are the residues of the active site from just before the characteristic HExxHxxGxxH motif through the MxP triad to the beginning of the S1′ loop.

To improve TACE potency and ultimately address selectivity over MMPs, lactams with a more flexible P1′ were synthesized. The 4-phenoxyphenyl analog **1b** increased pTACE potency to 185 nM. An even more flexible 4-benzyloxyphenyl P1′ group (**1c**) resulted in a 4 nM inhibitor of pTACE, greater than 3000-fold enhancement relative to **1a**. This suggested that the flexible benzyloxyphenyl P1′ can adopt the conformation necessary for good binding to TACE. **1c** remained potent for MMP-2 and -9, most likely because the benzyloxyphenyl group can also adopt a more linear conformation.

Further elaboration of the benzyl ether led to the discovery of 3,5-dimethylbenzyl as a TACE-selective P1′ group (**1d**) with 1000-, 1400-, and 400-fold selectivity for pTACE over MMP-1, -2, and -9, respectively. This exquisite selectivity appears to be largely due to steric effects, because replacement of the benzyl group with pyridinylmethyl (**1e**), quinolinylmethyl (**1f**), or a benzyl group having different substituents [1] had little effect on the selectivity profile. Substitution at both 3 and 5 positions of the benzyl ether is, however, required for good selectivity; monomethyl substitution (**1g**) is much less selective.

The TACE-selective P1′ groups were next incorporated into two series of potent MMP inhibitors reported in the literature. RS-113,456 (**2a**) was derived from a β-sulfonylhydroxamic acid and advanced to human clinical trials [J.A. Campbell et al., 1998, 216th Meeting of the Amer. Chem. Soc., abstract]. It was reported to be a subnanomolar inhibitor of MMP-2 and -9 (Table 1). Replacing the chlorophenoxy group of RS-113,456 with a (2,6-dimethyl-4-pyridinyl)methoxy P1′ decreased the affinity for MMP-2 and -9 by greater than 4000-fold (**2b**). Unfortunately, **2b** is only moderately active in pTACE, considerably less potent than the lactam analog **1e** (131 versus 14 nM). However, pTACE potency was greatly improved using a 4-quinolinylmethoxy group (**2c**), yielding a 4 nM inhibitor with excellent selectivity.

Prinomastat (**3a**) is another potent MMP inhibitor that advanced to development [23]. Incorporation of a 4-quinolinylmethoxy group to the thiomorpholine core of prinomastat provided a potent TACE inhibitor, **3b**. In contrast to the RS-113,456 series, **3b** is surprisingly active for the three MMPs, with $K_i$'s all under 100 nM. The (2,6-dimethyl-4-pyridinyl)methoxy analog **3c** attenuated the potency for MMPs ($K_i$ >250 nM) while modestly improving pTACE potency. Affinity for pTACE and selectivity were further enhanced using a (3,5-dimethoxyphenyl)methoxy P1′ group (**3d**). In both the RS-113,456 and prinomastat series, we demonstrated that by modifying the P1′ group alone, one can convert a potent MMP inhibitor to ones that are potent for pTACE and selective over all three MMPs tested.

In an attempt to design inhibitors structurally distinct from the prinomastat series, the sulfonyl group was first replaced by acetyl to give acetamide **4a**. We were delighted to find that **4a** remains potent for pTACE. Replacing the thiomorpholine ring of **4a** by piperidine (**4b**) yielded a pTACE inhibitor with good potency, albeit 7-fold less than **4a**. The pyrrolidine analog **4c** is even less potent. But in all cases, good selectivity over MMPs was maintained, again demonstrating effectiveness of the new P1′ groups.

The novel MMP-2 inhibitor **5a** incorporates a rationally designed benzothiadiazepine scaffold [24]. To improve its potency, the benzyloxy analog **5b** was synthesized. Surprisingly, it is less potent in the pTACE assay than **5a** (705 nM versus 274 nM), indicating a binding mode that differs somewhat from that of the previously described lactam series. The potency improved incrementally with dimethylbenzyloxy (**5c**) and substantially with a dimethoxybenzyloxy group (**5d**). We hypothesize that the bulky benzothiadiazepine scaffold induces a slight
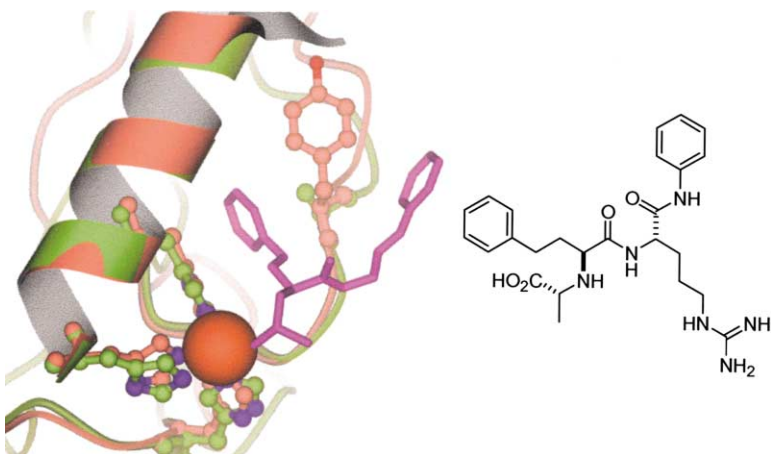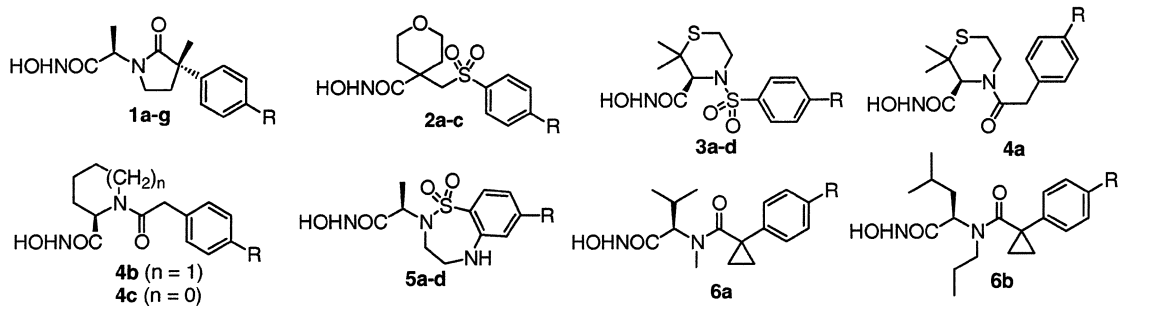


Figure 4. TACE Homology Model (Green) Superimposed on the Active Site of Inhibited MMP-3 (PDB File *1sln*; Light Red)

The catalytic zinc ion (orange) is coordinated by three histidine residues. Also shown is tyrosine 223 (light red) of MMP-3, which occupies the outer edge of the S1′ pocket, and the alanine (green), which replaces it in TACE. Inhibitor L-702,842 (from *1sln.pdb*) is depicted in purple. Other side chains, portions of the backbone of both proteins, and parts of the inhibitor are omitted for clarity. The figures were made with program MOLSCRIPT [35]. The chemical composition of the inhibitor, in approximately the same orientation as in the Figure, is shown to the right.

Table 1. In Vitro Profile of TACE Inhibitors

**1a-g**

**2a-c**

**3a-d**

**4a**

**4b** (n = 1)
**4c** (n = 0)

**5a-d**

**6a**

**6b**

| | R | pTACE (IC$_{50}$, nM)[a] | MMP-1 (K$_i$, nM) | MMP-2 (K$_i$, nM) | MMP-9 (K$_i$, nM) |
|---|---|---|---|---|---|
| **1a** | Phenyl | 13000 | 2288 | 82 | 35 |
| **1b** | Phenoxy | 185 | 143 | <3 | <2 |
| **1c** | benzyloxy | 4 | >5000 | 19 | 29 |
| **1d** | (3,5-dimethylphenyl)methoxy | 4 | 4747 | 5812 | 1634 |
| **1e** | (2,6-dimethyl-4-pyridinyl)methoxy | 14 | >5000 | 1585 | 688 |
| **1f** | (2-methyl-4-quinolinyl)methoxy | 1 | >5000 | 2050 | >3000 |
| **1g** | (3-methylphenyl)methoxy | 6 | >5000 | 18 | 6 |
| **2a**[b] | 4-chlorophenoxy | – | 590 | 0.22 | 0.58 |
| **2b** | (2,6-dimethyl-4-pyridinyl)methoxy | 131 | >5000 | 1744 | >2128 |
| **2c** | 4-quinolinylmethoxy | 4 | >5000 | 2282 | >2000 |
| **3a**[b] | 4-pyridinyloxy | – | 8 | 0.05 | 0.3 |
| **3b** | 4-quinolinylmethoxy | 10 | 56 | 57 | 88 |
| **3c** | (2,6-dimethyl-4-pyridinyl)methoxy | 6 | 1970 | 257 | 516 |
| **3d** | (3,5-dimethoxyphenyl)methoxy | 1 | 2272 | 423 | 630 |
| **4a** | (2-methyl-4-quinolinyl)methoxy | 2 | >5000 | 533 | 1106 |
| **4b** | (2-methyl-4-quinolinyl)methoxy | 15 | >5000 | >3000 | >2000 |
| **4c** | (2-methyl-4-quinolinyl)methoxy | 91 | >5000 | >3000 | >2000 |
| **5a** | methoxy | 274 | 1060 | 8 | 104 |
| **5b** | benzyloxy | 705 | >5000 | <3 | 4 |
| **5c** | 3,5-dimethylbenzyloxy | 229 | >5000 | 136 | >2000 |
| **5d** | 3,5-dimethoxybenzyloxy | 27 | >5000 | 491 | >2000 |
| **6a** | methoxy | 200 | 76 | 16 | 28 |
| **6b** | (2-methyl-4-quinolinyl)methoxy | 45 | >5000 | 491 | >2000 |

[a] Since semipurified pTACE was used in the routine assay, K$_i$ values were not determined for most of the compounds.
[b] The MMP data for compounds **2a** and **3a** were taken from the literature; no values for pTACE were determined.

adjustment of the TACE conformation. This may increase the energy and necessitate an even more bulky P1′ than in the other series in order to compensate. Perhaps the angle at which P1′ is presented also differs somewhat. Importantly, TACE selectivity was achieved with **5d** despite the conjectured difference in binding mode.

Another novel MMP inhibitor (**6a**) from our laboratory incorporates 1-phenyl-1-cyclopropanecarboxamide. The cyclopropane had been introduced by design in order to increase the population of conformers required for binding to MMPs. Once again, introduction of a TACE-selective P1′ group, in this case a 2-methyl-4-quinolinyl-methoxy group, not only improved activity for pTACE but also considerably improved selectivity over MMP-1, -2, and -9. The results with scaffold families **1–6** suggest not only the validity of the selectivity hypothesis, but also the transferability of selectivity from one scaffold to another by simple substitution of identical or very similar P1′ substituents.

**Computer Docking of Inhibitors**
We docked inhibitor **1c** into the active site of the TACE model using the protocol outlined in the Experimental

Procedures. The inhibitor was initially placed in the site "by hand" in an approximation to the presumed bound orientation, with the hydroxamate positioned to chelate the zinc ion in a bidentate fashion and with the intended P1′ moiety extending into S1′. After refinement by molecular dynamics (see Experimental Procedures), no substantial changes in the modeled TACE were apparent, and the ligand was oriented so that the oxygen atoms of the hydroxamic acid were about 2.0 Å distant from the zinc, and the carbonyl oxygen of the lactam formed hydrogen bonds with the amides of both L129 and G130 (Figure 5). We did not attempt docking to MMP-1 because of its foreshortened S1′ pocket, and crystal structures of MMP-2 and MMP-9 were not available. Because of the probabilistic nature of any homology model, particularly one with as many large insertions as the TACE one, no further docking into TACE of compounds was carried out.

Docking of **1c** and **1d** was, however, attempted with MMP-3 in the hope of elucidating reasons for selectivity against MMP-2 and -9, but we found that MMP-3 accommodates these P1′ chains adequately. The models suggest that **1c** and **1d** bind to MMP-3 with P1′ in an extended conformation, in contrast to the proposed
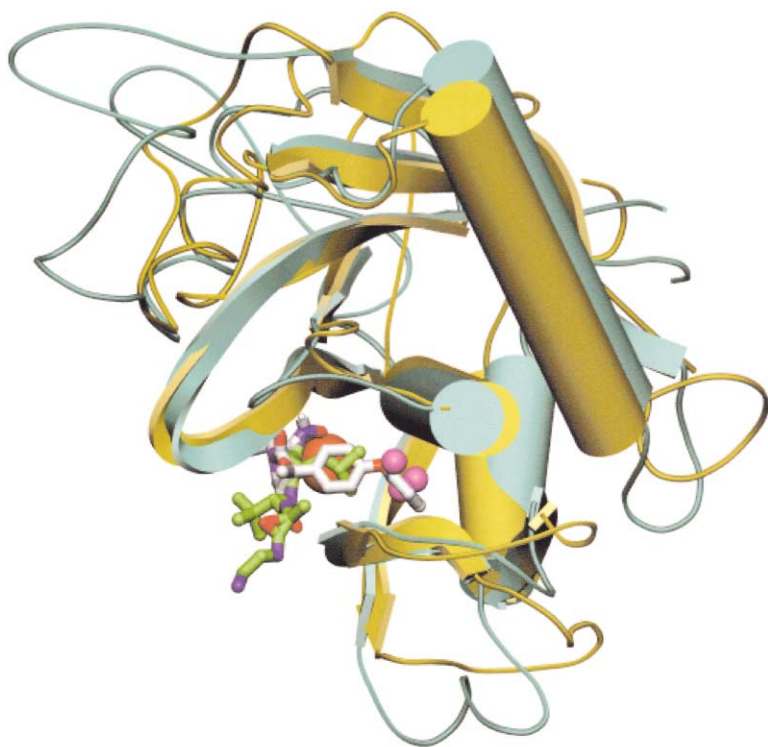
Figure 5. Superposition of the Inhibited TACE Crystal Structure onto a Computer Generated Complex of Molecule **3d** with the TACE Homology Model

The protein crystal structure is shown in cyan and its associated inhibitor in green. The homology model is colored yellow, and molecule **3d** is colored white. Zinc atoms are orange, and water molecules are magenta. Portions of the two protein structures for which the conformations overlay and the sequences correspond are depicted with cylinders and ribbons; regions where either the sequences or structures differ are represented as a thin cylindrical trace.

bent orientation in TACE (Figure 5). A subsequent assay with MMP-3 indicated that although **1d** is selective for TACE over MMP-3, activity is reduced by only about 30-fold (our unpublished data), indicating free energy differences too small to be perceived with these methods. In addition, it has been shown that flexibility and mobility of both protein and ligand can play a role by increasing the entropy of the system [25]. Screening against an extended set of enzymes will most likely be necessary to achieve a uniform selectivity profile.

Although we did not dock representative molecules from the other series into the TACE homology model, intuition suggests they bind similarly, as each contains a hydroxamic acid to coordinate zinc, an oxygen likely to form a hydrogen bond with amides of the β strand above the catalytic site, and a long and flexible P1′ substituent to occupy S1′.

**Comparison with Crystal Structure**

Recently, the crystal structure of TACE with a hydroxamic acid inhibitor became available (PDB file *1bkc*) [26], enabling evaluation of the accuracy of the homology model and computer docked structure. We were able to superimpose the α carbon atoms of 117 of the 255 residues of the model onto those of the TACE crystal structure with an rms deviation of 1.45 Å. The superimposed regions included all five strands of the characteristic β sheet, the MxP turn, and all three characteristic helices. A fourth helix, present in both TACE and reprolysin structures but not a feature of MMPs, was modeled with the wrong sequence of residues. As expected, the conformation of most loops differed considerably in the two structures. The superimposed structures are shown in Figure 5.

It is also of interest to examine the inhibitors in the two structures. The atoms of the hydroxamic acid moieties overlay well, and the methyne of the crystallographic inhibitor's P1′ isobutyl group is located in the center of the proximal ring of the modeled inhibitor's P1′. In addition, its distal ring is positioned at the location of three crystallographic water molecules. These observations indicate that the core of the homology model, selectivity hypothesis, and computer-docked inhibitor structure are all consistent with the crystallographically determined TACE/inhibitor complex.

**Significance**

**The central importance of TNF-α as an anti-inflammatory target has been well established by the therapeutic success of both anti-TNF-α antibody and TNFR II receptor fusion proteins. The zinc metalloenzyme TACE that processes this cytokine represents an attractive small-molecule target for medicinal research. Here we have described the steps leading to the development of inhibitors effective in TACE and selective with respect to a representative set of MMPs, MMP-1, -2, and -9.**

**Comparative modeling of TACE based on the structure of the snake venom protein atrolysin resulted in a plausible homology model. Careful inspection of the model and comparison with the crystal structure of inhibited MMP-3 suggested the S1′ pocket as a selectivity determinant for TACE. Examination of the periphery of this pocket highlighted a key residue difference—a tyrosine, conserved in all members of the MMP family, is replaced in TACE by the much smaller**

alanine, opening the side of the pocket and thus reinforcing the selectivity hypothesis.

By incorporation of appropriate P1′ substituents into a γ-lactam-derived hydroxamic acid inhibitor, we were able to achieve the desired selectivity. Transferability of the selectivity mechanism into five other series of inhibitors was then demonstrated by simple substitution at P1′. Computer modeling was used to dock a sample inhibitor into TACE in a convincing manner. Comparison with a subsequently determined X-ray crystal structure of inhibited TACE indicated our model to be consistent with the known structural information. Thus, despite inaccuracies on the periphery of the homology model, the fidelity of its protein core and substrate binding site enabled identification of the means of achieving specificity and, together with effective molecular design, the development of highly potent and selective compounds.

## Experimental Procedures

### Sequence Analysis

Sequence alignments were carried out using the GCG suite of programs (Wisconsin Package Version 8, Genetics Computer Group, Madison, WI): modules BestFit and Gap for pairwise and PileUp for multiple alignments. Sequences of the catalytic domains of MMP-1, -3, and -8 were extracted from Protein Data Bank files of their crystal structures (*1hfc*, *1sln*, and *1mnc*, respectively). The sequences of MMP-2 and MMP-9 were obtained from SWISS-PROT files *cog2_human* and *cog9_human* and aligned with the other MMPs in order to determine the approximate beginning and end residues of their catalytic domains. Similarly, the sequences of reprolysins adamalysin and atrolysin were taken from PDB files *1iag* and *1htd*, while those of jararhagin, trimerelysin, trigramin, and rhodostomin were obtained from SWISS-PROT (files *disj_botja, hr1b_trifl, disa_triga*, and *disr_agkrh*). The individual sequences were compared with each other and with the sequence of TACE, obtained from Ashok Amin at NYU. Alignments were generated for TACE with the set of reprolysins and with the set of MMPs, for the MMPs taken in pairs, for atrolysin versus adamalysin, and for TACE with atrolysin and with each of the individual MMPs. The alignment of atrolysin with TACE was further modified during the homology-building stage (*vide supra*).

### Homology Modeling

Many homology models of TACE were made in the course of this work. At the outset models were built using XLOOK (LOOK, version 3, Molecular Applications Group, Palo Alto, CA). Each model was inspected for conformance to conventional principles of protein architecture (for example charged and polar residues should be located predominantly on exposed faces of β sheets, on polar sides of amphiphilic helices, or in loops). Sequence alignments were then adjusted and new models created.

The alignment used in homology modeling was further optimized in order to maximize sequence similarity in segments corresponding to secondary structural elements of the homolog's crystal structure. At later stages of model-building, we attempted to optimize the conformation of short loops (fewer than 8 residues) using procedure FRAGLE (FRAGment Locate and Extract) [27], which presents to the user a choice of fragments from well-refined protein structures whose end residues possess backbone conformations which match those of residues immediately preceding and following the loop to be inserted.

### Molecular Modeling

Molecular surfaces were calculated with program GRASP [28], and the program PSSHOW [29] was used for visualization of molecular structure. Docking of inhibitors was carried out using Bforce [30], a modified version of AMBER [31] that uses a mobile ligand and active site, and a fixed "bulk" consisting of the rest of the protein

and represented implicitly by points of a grid. Force field parameters for the ligands were assembled from the AMBER atomic parameter list, and charges were calculated using MOPAC [32] and the AM1 Hamiltonian. Inhibitors were initially docked "by hand," and the systems were then energy minimized and refined by short (20 ps) runs of molecular dynamics. During the simulations, distances between zinc and $N\epsilon$ atoms of the chelating histidine residues, and between zinc and $O\epsilon$ atoms of the catalytic site Glu, were constrained to 2.1 and 4.8 Å, respectively (the values are close to those appearing in crystal structures of MMPs), with a force constant of 10.0 kcal/mol·Å$^2$. In molecular dynamics runs of the TACE model, atoms of the main chain were constrained to their positions in the starting structure using a very weak harmonic force constant of 0.5 kcal/mol·Å$^2$. No constraints were imposed on the ligand, which was completely free to move. As in previous work with thermolysin [33], the hydroxamic acid was charged, and the catalysic site Glu was protonated. The final step was minimization of the average structure computed over the last 3 ps of simulation.

### Inhibitor Synthesis and Testing

Synthesis of inhibitors **1a–1g** in enantiomerically pure form was described in reference [1]. Experimental details for inhibitors **2b–2c** and **6a–6b** were disclosed in previously published patent applications WO9958528 and WO0059874. Description of synthesis and full experimental details of **5a–5d** will be reported elsewhere [24]. Inhibitors **3b–3d** were synthesized following the sequence described below. Compounds **4a–4c** were prepared using conditions analogous to those for **3c**.

Due to the fact that US patent 5,830,742 covers the usage of truncated human TACE, we used semipurified TACE from porcine spleen as the primary assay. According to both the TACE homology model and the subsequently determined crystal structure, no non-conserved residues abut the proposed inhibitor binding site, suggesting pTACE as a suitable substitute for human enzyme. Counter-screen assays included MMP-2 and -9 as representative members having deep S1′ sites and MMP-1 as a representative with shallow S1′. Details of these assays are described in a previous publication [34].

### Synthesis of Hydroxamic Acids 3b–3d

4-Hydroxybenzenesulfonyl chloride (0.41 g, 0.22 mmol) in methylene chloride (1 ml) was added dropwise to methyl (*S*)-2,2-dimethyl-3-thiomorpholinecarboxylate (0.37 g, 0.20 mmol) in pyridine (4 ml) at room temperature. After stirring for 30 min, the solvent was removed and the residue taken up in ethyl acetate-water (1:1, 20 ml). The mixture was extracted with ethyl acetate (3×), and the combined extracts were washed with 10% citric acid (2×), water, and brine, dried over MgSO₄, and concentrated. The residue was purified by flash chromatography (silica gel, 50% ethyl acetate:hexane) to provide methyl (S)-4-[(4-hydroxyphenyl)sulfonyl]-2,2-dimethyl-3-thiomorpholinecarboxylate (249 mg, 37%) as a light yellow solid: ¹H NMR (300 MHz, CDCl₃) δ 7.60 (m, 2H), 6.88 (m, 2H), 5.71 (s, 1H), 4.41 (s, 1H), 4.06 (dt, 1H, J = 2.7, 11.7 Hz), 3.75 (dt, 1H, J = 2.9, 12.8 Hz), 3.43 (s, 3H), 3.13 (m, 1H), 2.46 (dt, 1H, J = 2.6, 12.9 Hz), 1.62 (s, 3H), 1.27 (s, 3H); MS (ESI) *m/z* 344 (M−H)⁻.

Cesium carbonate (396 mg, 1.22 mmol) was added in one portion to the phenol obtained from the previous step (140 mg, 0.41 mmol), sodium iodide (79 mg, 0.53 mmol), and 4-chloromethyl-2,6-dimethylpyridine hydrochloride (101 mg, 0.53 mmol) in anhydrous DMSO (4 ml) at room temperature. The mixture was stirred for 2.5 hr and then diluted with water and extracted with ethyl acetate (3×). The combined organic layers were washed with water (2×) and brine, dried over MgSO₄, and concentrated. The residue was purified by flash chromatography (silica gel, 50% to 80% ethyl acetate:hexane) to provide methyl (S)-4-[[4-[(2,6-dimethyl-4-pyridinyl)methoxy]phenyl]sulfonyl]-2,2-dimethyl-3-thiomorpholinecarboxylate (157 mg, 82%) as a waxy white solid: ¹H NMR (300 MHz, CDCl₃) δ 7.65 (m, 2H), 6.98 (m, 2H), 5.07 (s, 2H), 4.41 (s, 1H), 4.05 (m, 1H), 3.74 (m, 1H), 3.36 (s, 3H), 3.11 (m, 1H), 2.54 (s, 6H), 2.46 (m, 1H), 1.62 (s, 3H), 1.27 (s, 3H); MS (ESI) m/z 465 (M+H)⁺.

The ester obtained from the previous step was heated to reflux in 6 N HCl (10 ml) for 15 hr. The solvent was removed in vacuo, and the residue was dried by evaporation with toluene (2×) and

chloroform (2×). This provided (S)-4-[[4-[(2,6-dimethyl-4-pyridinyl)methoxy]phenyl]sulfonyl]-2,2-dimethyl-3-thiomorpholinecarboxcylic acid as a brittle foam that was taken to the next step without further purification: $^1$H NMR (300 MHz, CD$_3$OD) δ 7.77 (s, 2H), 7.72 (d, 2H, J = 8.8 Hz), 7.18 (d, 2H, J = 8.8 Hz), 5.42 (s, 2H), 4.34 (s, 1H), 3.97 (m, 1H), 3.73 (dt, 1H, J = 2.6, 12.5 Hz), 3.04 (dt, 1H, J = 3.7, 13.2 Hz), 2.75 (s, 6H), 2.43 (m, 1H), 1.54 (s, 3H), 1.30 (s, 3H); MS (ESI) m/z 451 (M+H)$^+$.

Diisopropyl ethyl amine (440 mg, 3.4 mmol) was added dropwise to the acid from the previous step (0.34 mmol), BOP reagent (165 mg, 0.37 mmol), and hydroxylamine hydrochloride (71 mg, 1.02 mmol) in DMF (3 ml) at room temperature. The mixture was stirred overnight and the solvent removed in vacuo. Purification by reverse-phase HPLC (acetonitrile:water) provided (S)-4-[[4-[(2,6-dimethyl-4-pyridinyl)methoxy]phenyl]sulfonyl]-N-hydroxy-2,2-dimethyl-3-thiomorpholinecarboxamide **3c** (65 mg, 33%) as a fluffy white powder after lyophilization: $^1$H NMR (300 MHz, DMSO) δ 7.71 (m, 4H), 7.15 (m, 2H), 5.40 (m, 2H), 4.07 (s, 1H), 3.88 (m, 1H), 3.34 (m, 1H), 3.07 (m, 1H), 2.72 (s, 6H), 2.43 (m, 1H), 1.54 (s, 3H), 1.20 (s, 3H); MS (ESI) m/z 466 (M+H)$^+$; HRMS calculated for (C$_{21}$H$_{27}$N$_3$O$_5$S$_2$ + H)$^+$ 466.1470, found 466.1468.

(S)-N-hydroxy-2,2-dimethyl-4-[[4-(4-quinolinylmethoxy)phenyl]sulfonyl]-3-thiomorpholinecarboxamide (**3b**) was made using an analogous procedure to compound **3c**, substituting 4-chlormethylquinoline for 4-chloromethyl-4,6-dimethylpyridine. $^1$HNMR (300 MHz, DMSO) δ 8.96 (d, 1H, J = 4.7 Hz), 8.21 (d, 1H, J = 8.4 Hz), 8.08 (d, 1H, J = 8.4 Hz), 7.85 (t, 1H, J = 7.0 Hz), 7.73 (m, 2H), 7.63 (d, 2H, J = 8.8 Hz), 7.26 (d, 2H, J = 8.8 Hz), 5.78 (s, 2H), 3.99 (s, 1H), 3.88 (m, 1H), 3.69 (m, 1H), 2.81 (m, 1H), 2.43 (m, 1H), 1.35 (s, 3H), 1.11 (s, 3H); MS (ESI) m/z 488 (M+H)$^+$; HRMS calculated for (C$_{23}$H$_{25}$N$_3$O$_5$S$_2$ + H)$^+$ 488.1301, found 488.1300.

(S)-4-[[4-[(3,5-Dimethoxyphenyl)methoxy]phenyl]sulfonyl]-N-hydroxy-2,2-dimethyl-3-thiomorpholinecarboxamide(**3d**) was made in an analogous procedure to compound **3c**, substituting 3,5-dimethoxybenzylchloride for 4-chloromethyl-4,6-dimethylpyridine: $^1$H NMR (300 MHz, DMSO) δ 7.54 (d, 2H, 8.8 Hz), 7.10 (d, 2H, 8.8 Hz), 6.58 (s, 2H), 6.43 (s, 1H), 5.08 (s, 2H), 3.99 (s, 1H), 3.91 (m, 1H), 3.71 (s, 6H), 3.32 (m, 1H), 2.81 (m, 1H), 2.42 (m, 1H), 1.36 (s, 3H), 1.13 (s, 3H); MS (ESI) m/z 519 (M+Na)$^+$; HRMS calculated for (C$_{22}$H$_{28}$N$_2$O$_7$S$_2$ + H)$^+$ 497.1417, found 497.1422.

## References

1. Duan, J.J.-W., Chen, L., Wasserman, Z.R., Lu, Z., Liu, R.-Q., Covington, M.B., Qian, M., Hardman, K.D., Magolda, R.L., Newton, R.C., et al. (2002). Discovery of γ-lactam hydroxamic acids as selective inhibitors of tumor necrosis factor α converting enzyme: design, synthesis, and structure-activity relationships. J. Med. Chem. 45, 4954–4957.

2. Elliott, M.J., Maini, R.N., Feldmann, M., Kalden, J.R., Antoni, C., Smolen, J.S., Leeb, B., Breedveld, F.C., Macfarlane, J.D., Bijl, H., et al. (1994). Randomised double-blind comparison of chimeric monoclonal antibody to tumour necrosis factor alpha (cA2) versus placebo in rheumatoid arthritis. Lancet 344, 1105–1110.

3. Lipsky, P.E., van der Heijde, D.M., St Clair, E.W., Furst, D.E., Breedveld, F.C., Kalden, J.R., Smolen, J.S., Weisman, M., Emery, P., Feldmann, M., et al. (2000). Infliximab and methotrexate in the treatment of rheumatoid arthritis. N. Engl. J. Med. 343, 1594–1602.

4. Moreland, L.W., Baumgartner, S.W., Schiff, M., Tindall, E.A., Fleischmann, R.M., Weaver, A.L., Ettlinger, R.E., Cohen, S., Koopmam, W.J., Mohler, K., et al. (1997). Treatment of rheumatoid arthritis with a recombinant human tumor necrosis factor receptor (p75)-Fc fusion protein. N. Engl. J. Med. 337, 141–147.

5. Newton, R.C., and Decicco, C.P. (1999). Therapeutic potential and strategies for inhibiting tumor necrosis factor-alpha. J. Med. Chem. 42, 2295–2314.

6. Gearing, A.J.H., Beckett, P., Christodoulou, M., Churchill, M., Clements, J., Davidson, A.H., Drummond, A.H., Galloway, W.A.,

Gilbert, R., Gordon, J.L., et al. (1994). Processing of tumor necrosis factor-alpha precursor by metalloproteinases. Nature 370, 555–557.

7. Black, R.A., Rauch, C.T., Kozlosky, C.J., Peschon, J.J., Slack, J.L., Wolfson, M.F., Castner, B.J., Stocking, K.L., Reddy, P., Srinivasan, S., et al. (1997). A metalloproteinase disintegrin that releases tumor-necrosis factor-alpha from cells. Nature 385, 729–733.

8. Moss, M.L., Jin, S.L.C., Milla, M.E., Burkhart, W., Carter, H.L., Chen, W.-J., Clay, W.C., Didsbury, J.R., Hassler, D., Hoffman, C.R., et al. (1997). Cloning of a disintegrin metalloproteinase that processes precursor tumor-necrosis factor-alpha. Nature 385, 733–736.

9. Wojtowicz-Praga, S., Torri, J., Johnson, M., Steen, V., Marshall, J., Ness, E., Dickson, R., Sale, M., Rasmussen, H.S., Chiodo, T.A., et al. (1998). Phase I trial of marimastat, a novel matrix metalloproteinase inhibitor, administered orally to patients with advanced lung cancer. J. Clin. Oncol. 16, 2150–2156.

10. Scatana, R. (2000). Prinomastat, a hydroxamate-based matrix metalloproteinase inhibitor. A novel pharmacological approach for tissue remodelling-related diseases. Exp. Opin. Investig. Drugs 9, 2159–2165.

11. Levitt, N.C., Eskens, F.A., O'Byrne, K.J., Propper, D.J., Denis, L.J., Owen, S.J., Choi, L., Foekens, J.A., Wilner, S., Wood, J.M., et al. (2001). Phase I and pharmacological study of the oral matrix metalloproteinase inhibitor, MMI270 (CGS27023A), in patients with advanced solid cancer. Clin. Cancer Res. 7, 1912–1922.

12. Nelson, F.C., and Zask, A. (1999). The therapeutic potential of small molecule TACE inhibitors. Exp. Opin. Investig. Drugs 8, 383–392.

13. Nagase, H., Barrett, A.J., and Woessner, J.F., Jr. (1992). Nomenclature and glossary of the matrix metalloproteinases. Matrix Suppl. 1, 421–424.

14. Schechter, I., and Berger, A. (1967). On the size of the active site in proteases. I. Papain. Biochem. Biophys. Res. Commun. 27, 157–162.

15. Bode, W., and Maskos, K. (2001). Structural studies on MMPs and TIMPs. Methods Mol. Biol. 151, 45–77.

16. Dhanaraj, V., Ye, Q.Z., Johnson, L.L., Hupe, D.J., Ortwine, D.F., Dunbar, J.B., Jr., Rubin, J.R., Pavlovsky, A., Humblet, C., and Blundell, T.L. (1996). X-ray structure of a hydroxamate inhibitor complex of stromelysin catalytic domain and its comparison with members of the zinc metalloproteinase superfamily. Structure 4, 375–386.

17. Zhang, D., Botos, I., Gomis-Rueth, F.-X., Doll, R., Blood, C., Njoroge, F.G., Fox, J.W., Bode, W., and Meyer, E.F. (1994). Structural interaction of natural and synthetic inhibitors with the venom metalloproteinase, atrolysin C (form d). Proc. Natl. Acad. Sci. USA 91, 8447–8451.

18. Gomis-Rueth, F.X., Kress, L.F., and Bode, W. (1993). First structure of a snake venom metalloproteinase: a prototype for matrix metalloproteinases/collagenases. EMBO J. 12, 4151–4157.

19. Gomis-Ruth, F.X., Meyer, E.F., Kress, L., and Politi, V. (1998). Structures of adamalysin II with peptidic inhibitors. Implications for the design of tumor necrosis factor alpha convertase inhibitors. Protein Sci. 7, 283–292.

20. Cherney, R.J., Decicco, C.P., Nelson, D.J., Wang, L., Meyer, D.T., Hardman, K.D., Copeland, R.A., and Arner, E.C. (1997). Potent carboxylate inhibitors of stromelysin containing P2′ piperazic acids and P1′ biaryl moieties. Bioorg. Med. Chem. Lett. 7, 1757–1762.

21. Browner, M.F., Smith, W.W., and Castelhano, A.L. (1995). Matrilysin-inhibitor complexes: common themes among metalloproteases. Biochemistry 34, 6602–6610.

22. Gooley, P.R., O'Connell, J.F., Marcy, A.I., Cuca, G.C., Salowe, S.P., Bush, B.L., Hermes, J.D., Esser, C.K., Hagmann, W.K., Springer, J.P., et al. (1994). The NMR structure of the inhibited catalytic domain of human stromelysin-1. Nat. Struct. Biol. 1, 111–118.

23. Scatena, R. (2000). Prinomastat, a hydroxamate-based matrix metalloproteinase inhibitor. A novel pharmacological approach for tissue remodelling-related diseases. Expert Opin. Investig. Drugs 9, 2159–2165.

24. Cherney, R.J., Duan, J.J.-W., Voss, M.E., Chen, L., Wang, L., Meyer, D.T., Wasserman, Z.R., Hardman, K.D., Liu, R.Q., Covington, M.B., et al. (2003). Design, synthesis, and evaluation of benzothiadiazepine hydroxamates as selective tumor necrosis factor-$\alpha$ converting enzyme (TACE) inhibitors. J. Med. Chem., in press.

25. Moy, F.J., Chanda, P.K., Chen, J., Cosmi, S., Edris, W., Levin, J.I., Rush, T.S., Wilhelm, J., and Powers, R. (2002). Impact of mobility on structure-based drug design for the MMPs. J. Am. Chem. Soc. *124*, 12658–12659.

26. Maskos, K., Fernandez-Catalan, C., Huber, R., Bourenkov, G.P., Bartunik, H., Ellestad, G.A., Reddy, P., Wolfson, M.F., Rauch, C.T., Castner, B.J., et al. (1998). Crystal structure of the catalytic domain of human tumor necrosis factor-alpha-converting enzyme. Proc. Natl. Acad. Sci. USA *95*, 3408–3412.

27. Finzel, B.C., Kimatian, S., Ohlendorf, D.H., Wendoloski, J.J., Levitt, M., and Salemme, F.R. (1990). Molecular modeling with substructure libraries derived from known protein structures. In Crystallographic and Modeling Methods in Molecular Design, C.E. Bugg and S.E. Ealick, eds. (New York: Springer-Verlag), pp. 175–188.

28. Nicholls, A., Sharp, K.A., and Honig, B. (1991). Protein folding and association: insights from the interfacial and thermodynamic properties of hydrocarbons. Proteins *11*, 281–296.

29. Swanson, E. (1996). PSSHOW User's Guide, 2.2 Edition.

30. Luty, B.A., Wasserman, Z.R., Stouten, P.F.W., Hodge, C.N., Zacharias, M., and McCammon, J.A. (1995). A molecular mechanics/grid method for evaluation of ligand-receptor interactions. J. Comput. Chem. *16*, 454–464.

31. Weiner, P.K., and Kollman, P.A. (1981). AMBER: assisted model building with energy refinement. A general program for modeling molecules and their interactions. J. Comput. Chem. *2*, 287–303.

32. Stewart, J.J. (1990). A general molecular orbital package. In MOPAC Manual, Sixth Edition.

33. Wasserman, Z.R., and Hodge, C.N. (1996). Fitting an inhibitor into the active site of thermolysin: a molecular dynamics case study. Proteins *24*, 227–237.

34. Xue, C.-B., Voss, M.E., Nelson, D.J., Duan, J.J.-W., Cherney, R.J., Jacobson, I.C., He X., Roderick J., Chen L., Corbett R.L., et al. (2001). Design, synthesis, and structure-activity relationships of macrocyclic hydroxamic acids that inhibit tumor necrosis factor alpha release in vitro and in vivo. J. Med. Chem. *44*, 2636–2660.

35. Kraulis, P.J. (1991). MOLSCRIPT: a program to produce both detailed and schematic plots of protein structures. J. Appl. Crystallogr. *24*, 945–949.